J Electr Eng Technol.2018; 13(3): 1326-1336
http://doi.org/10.5370/JEET.2018.13.3.1326

ISSN(Print) 1975-0102
ISSN(Online) 2093-7423

A Numerical Approach for Lightning Impulse Flashover Voltage Prediction of Typical Air Gaps

Zhibin Qiu†, Jiangjun Ruan*, Congpeng Huang*, Wenjie Xu* and Daochun Huang*

Abstract – This paper proposes a numerical approach to predict the critical flashover voltages of air gaps under lightning impulses. For an air gap, the impulse voltage waveform features and electric field features are defined to characterize its energy storage status before the initiation of breakdown. These features are taken as the input parameters of the predictive model established by support vector machine (SVM). Given an applied voltage range, the golden section search method is used to compute the prediction results efficiently. This method was applied to predict the critical flashover voltages of rod-rod, rod-plane and sphere-plane gaps over a wide range of gap lengths and impulse voltage waveshapes. The predicted results coincide well with the experimental data, with the same trends and acceptable errors. The mean absolute percentage errors of 6 groups of test samples are within 4.6%, which demonstrates the validity and accuracy of the predictive model. This method provides an effectual way to obtain the critical flashover voltage and might be helpful to estimate the safe clearances of air gaps for insulation design.

Keywords: Air gap, Flashover voltage prediction, Lightning impulse, Electric field features, Impulse voltage waveform, Support vector machine (SVM), Golden section search method.

1. Introduction

High voltage technology is a traditional discipline mainly based on experimental studies. It has been a long sought goal for researchers and engineers to study dielectric discharge characteristics and mechanisms by mathematical calculations instead of costly and long-periodic experimental tests. Air is the most common and important insulation media in power systems, its discharge characteristics are the basis of external insulation design in transmission and transformation projects. In China, driven by the rapid development of ultra-high voltage (UHV) transmission technology [1], in-depth studies have been carried out on long air gap discharge in the past few years [2-3], both experimentally and theoretically. Recently, some scholars propose an innovative research concept called "computational high voltage engineering," aiming at solving perplexing issues of high voltage and insulation technology by simulations rather than experiments. Prediction of air gap breakdown characteristics, especially the flashover voltage, is one of the important issues to be studied in this new discipline system.

Up to now, numerous mathematical models have been put forward to describe the physical processes of both positive [4, 5] and negative discharge [6-8]. These models contribute to better understanding the development process and the mechanism of air discharge, and might be helpful to predict the flashover voltages of air gaps. However, due to the complexity of air discharge, most of the existing physical models are based on some simplifications or assumptions, which may lead to some errors between the predicted and experimental results. In fact, air discharge can be viewed as a complex movement system involving various particles, such as electrons, ions, photons, atoms, etc., and the discharge process is accompanied by complicated electrical, optical and thermal phenomena. Since the particle movement is affected by numerous factors and the discharge is a fast transient process with large dispersion, it is very difficult to establish a scientific model to accurately simulate the evolution of the successive phases during the whole discharge process.

Air discharge begins with gas ionization, which results from the interaction of the particles in air with an applied electric field [9]. The temporal and spatial variations of the electric field directly influence the formation and development of streamer and leader, finally affect the breakdown voltage of the air gap. Since the electric field distribution is time-varying during the discharge propagation, it is difficult to simulate the temporal process so as to predict the flashover voltage. From another perspective without regard to the discharge process, gas breakdown can be viewed as conversion of the capacitive energy stored in the electric field to thermal energy, along with the conversion of the discharge channel from an insulation state to conductive plasma [10]. Hence, it can be assumed that the flashover voltage of an air gap correlates to its energy storage status before initiation of breakdown. If we can

† Corresponding Author: School of Electrical Engineering, Wuhan University, China. (whuerliuming@whu.edu.cn)
* School of Electrical Engineering, Wuhan University, China. (ruan308@126.com, {1649672039, 1789965541}@qq.com, huangdc99@163.com)
Received: June 12, 2017; Accepted: January 7, 2018

establish the relationship between the flashover voltage with the temporal accumulation and spatial distribution of the electric field energy before corona inception, it may be useful to predict the breakdown voltages of air gaps with various geometries and subjected to different voltage shapes, helping to reduce laboratory experiments.

The electric field of an air gap under an applied voltage can be characterized by two sets of parameters [9]: (1) the static electric field which defines the spatial distribution of the electric field, determined by the electrode structures, gap length and the distance from the ground or surroundings, and (2) the voltage waveshape which defines the temporal variation of the electric field. The existing models usually take the gap geometry and the voltage waveshape as the input data, which are difficult to consider complicated gap configurations, since their structure cannot be described by some simple geometric parameters. It is more appropriate to characterize the gap configurations by spatial electric field distribution instead of some geometric parameters.

In this paper, a numerical approach is proposed for lightning impulse voltage prediction of air gaps. The impulse voltage waveform features are firstly proposed to define the lightning impulse voltage wave, together with the electric field features [11-14], they are taken as the input data of the model. The predictive model is established by support vector machine (SVM), a machine learning algorithm with good performance in solving small sample and multi-dimensional nonlinear problems. The SVM model establishes the multi-dimensional nonlinear relationship between the energy storage features and the flashover voltage, and therefore we need not treat the complex and random physical processes directly. The golden section search method is introduced to this method to improve the computational efficiency. Given an applied voltage range, the model can quickly predict the flashover voltage when the stopping criterion for iteration is satisfied. The implementation procedure of this model is introduced in detail. The proposed method was applied to predict the flashover voltages of air gaps with various configurations and subjected to different lightning impulse waveforms. The predicted results were compared with the experimental data to validate the validity of this approach.

2. Energy Storage Features of Air Gaps

Air discharge must be caused by some macro factors which can be summarized as applied voltage waveform, electric field distribution and atmospheric environment. The flashover voltage results from the comprehensive function of the three factors. Since the atmospheric correction methods are already available and have been proven to be effective, the atmospheric parameters are not considered in the present paper. The applied voltage waveform can be obtained by measuring devices or simulated by computers. It can be characterized by some features like voltage amplitude, voltage duration, rising steepness of the wave and voltage integral, etc. The electric field distribution of an air gap can be calculated by finite element method (FEM), and can be characterized by some features such as electric field strength, field energy, field gradient, field inhomogeneity, etc. The applied impulse voltage waveform and the electric field distribution respectively characterize the temporal and spatial variations of the energy applied on an air gap. These features are collectively called energy storage features in this paper.

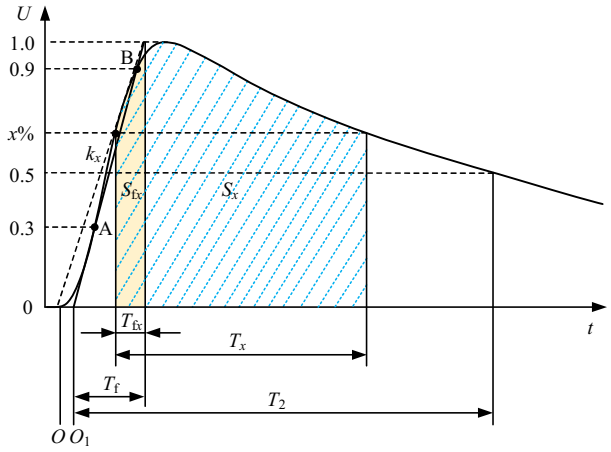

Fig. 1. Definitions of partial impulse voltage waveform features

2.1 Impulse voltage waveform features

The full lightning impulse voltage wave is shown in Fig. 1 [15], which can be approximately simulated by a double exponential function. The full wave expression is

$$u(t) = A(\mathrm{e}^{-\alpha t} - \mathrm{e}^{-\beta t}) \tag{1}$$

A is the amplitude coefficient, α and β are respectively the reciprocal of wave tail and wave front constant. The three parameters are usually unknown coefficients.

According to the definition of lightning impulse voltage waveform, set the front time and the time to half-value are T_f and T_2, and the corresponding moments of virtual origin O_1 and voltage peak are T_0 and T_m, there are five constraints for lightning impulse wave: (1) the voltage value at the moment of T_m is the crest voltage U_{max}; (2) the voltage value at the moment of T_0+T_2 is $0.5U_{max}$; (3) the voltage value at the moment of T_0+$0.3T_f$ is $0.3U_{max}$; (4) the voltage value at the moment of T_0+$0.9T_f$ is $0.9U_{max}$; (5) the derivative of $u(t)$ at the moment of T_m is 0. These constraints can be expressed as follows:

$$u(T_m) = A(\mathrm{e}^{-\alpha T_m} - \mathrm{e}^{-\beta T_m}) = U_{max}$$
$$u(T_0 + T_2) = A(\mathrm{e}^{-\alpha(T_0+T_2)} - \mathrm{e}^{-\beta(T_0+T_2)}) = 0.5U_{max}$$

$$u(T_0+0.3T_f)=A(e^{-\alpha(T_0+0.3T_f)}-e^{-\beta(T_0+0.3T_f)})=0.3U_{max} \quad (2)$$
$$u(T_0+0.9T_f)=A(e^{-\alpha(T_0+0.9T_f)}-e^{-\beta(T_0+0.9T_f)})=0.9U_{max}$$
$$\left.\frac{du}{dt}\right|_{t=T_m}=A(\beta e^{-\beta T_m}-\alpha e^{-\alpha T_m})=0$$

The lightning impulse voltage waveform is usually described by known U_{max}, T_f and T_2. By solving the nonlinear Eqs. (2) using the least square method, the three unknown parameters A, α and β can be obtained.

According to the characteristics of the impulse voltage waveform and its effect on the breakdown of air gaps, the following 5 basic features are defined and used to characterize the global properties of the impulse voltage waveform.

(1) The maximum value of the impulse voltage U_{max}. It characterizes the upper limit of the energy applied on the air gap.

$$U_{max}=\max(u(t)) \quad (3)$$

(2) Time features, including the front time T_f and the time to half-value T_2. These two features respectively describe the rise time and duration time of the impulse voltage waveform.

(3) The average rate of rise du/dt, which means the slope of the best fitting straight line between $0.3U_{max}$ and $0.9U_{max}$. This feature characterizes the steepness or the rise speed of the impulse voltage waveform.

$$\frac{du}{dt}=\frac{U_{max}}{T_f} \quad (4)$$

(4) Voltage integral S, which means the integral of the impulse voltage waveform with respect to time, also can be described by the curved surface area under the voltage waveform. The voltage integral characterizes the accumulative effect of the applied energy on the gap breakdown.

$$S=\int_0^{+\infty}u(t)dt \quad (5)$$

In addition to the above-mentioned 5 basic features, the following additional features are defined to characterize the local properties of the impulse voltage waveform.

(1) The slope at the moment of $x\%U_{max}$, called k_x.

$$k_x=\left.\frac{du}{dt}\right|_{t=t_x} \quad (6)$$

where t_x is the moment when the impulse voltage rises to $x\%U_{max}$ during the wave front.

(2) The time interval T_x for which the impulse voltage exceeds $x\%U_{max}$.

$$T_x=t'_x-t_x \quad (7)$$

where t'_x is the moment when the impulse voltage falls to $x\%U_{max}$ during the wave tail.

(3) The time interval T_{fx} for which the impulse voltage exceeds $x\%U_{max}$ during the wave front.

$$T_{fx}=T_f-t_x \quad (8)$$

(4) The voltage integral S_x over the time interval T_x.

$$S_x=\int_{t_x}^{t'_x}u(t)dt \quad (9)$$

(5) The voltage integral S_{fx} over the time interval T_{fx}.

$$S_{fx}=\int_{t_x}^{T_f}u(t)dt \quad (10)$$

In this paper, x% includes 90%, 75% and 60%, hence, there are altogether 15 additional voltage waveform features. k_x is the feature to characterize the rising steepness of the waveform, T_x and T_{fx} are time features, S_x and S_{fx} are voltage integral features. The definitions of partial impulse voltage waveform features are shown in Fig. 1.

2.2 Electric field features

For a given air gap, the discharge processes vary every time even under the same applied lightning impulse waveform and the same atmospheric environment. However, the dispersion of the discharge voltage can be kept in a certain range, and the electric field distribution before the initiation of streamer discharge will also not change. In this paper, the electric field features in the discharge channel and along the shortest discharge path of an air gap are extracted from the finite element calculation results of the electric field distribution, and used to characterize the gap geometry. The discharge channel is defined artificially as an area between the high-voltage and grounded electrodes, and the shortest discharge path is the inter-electrode path along which the distance between two electrodes is the shortest. In this paper, several features are defined to characterize the electric field distribution of an air gap, which are divided into 4 groups.

(1) Electric field strength E_m and E_a, respectively mean the maximum and average values of the field strength in the discharge channel.

$$E_m=\max E_i \quad (i=1,2,\cdots,n) \quad (11)$$
$$E_a=\sum_{i=1}^{n}E_i/n \quad (12)$$

where E_i is the electric field strength of the ith element of

the FEM model in the discharge channel, and n is the total number of the elements.

(2) Electric field energy W and energy density W_d in the discharge channel.

$$W = \sum_{i=1}^{n} W_i = \sum_{i=1}^{n} (\frac{1}{2} \varepsilon_0 E_i^2 V_i) \tag{13}$$

$$W_d = W / \sum_{i=1}^{n} V_i \tag{14}$$

where W_i and V_i are respectively the energy and volume of the ith element, and ε_0 is the vacuum permittivity.

(3) Electric field gradient E_{gm} and E_{ga}, respectively mean the maximum and average values of the field gradient along the shortest discharge path.

$$E_{gm} = \max(|-\text{grad}E_i|) \quad (i = 1, 2, ..., n) \tag{15}$$

$$E_{ga} = \frac{1}{n} \sum_{i=1}^{n} (|-\text{grad}E_i|) \tag{16}$$

where the | | represents the absolute value sign.

(4) Electric field distortion factor E_d in the discharge channel and some scaling parameters related to the field strength, field energy and field gradient, including V_{rx}, W_{rx}, L_{rx}. V_{rx} and W_{rx} respectively mean the volume and energy ratio of the region whose field strength exceeds $x\%E_m$. L_{rx} is the length ratio of the path on which the field gradient exceeds $x\%E_{gm}$. $x\%$ include 90%, 75%, 50% and 25%. These features characterize the inhomogeneity of the electric field and energy distribution in the gap.

$$E_d = (E_m - E_a) / E_a \tag{17}$$

$$V_{rx} = \sum_{j=1}^{m} V_j / \sum_{i=1}^{n} V_i \tag{18}$$

$$W_{rx} = \sum_{j=1}^{m} W_j / W \tag{19}$$

$$L_{rx} = L_x / d \tag{20}$$

V_j and W_j are the volume and energy of the jth element in the discharge channel whose electric field strength exceeds $x\%E_m$, and m is the total number of these elements. L_x is the length of the path on which the electric field gradient exceeds $x\%E_{gm}$, and d is the gap distance.

The aforementioned features describe the electric field and energy storage status of an air gap from different aspects, including the magnitude, distribution and inhomogeneity. The energy storage features, including 20 impulse voltage waveform features and 19 electric field features were taken as the input of the SVM model.

3. Predictive Model

The predictive model is established by SVM, a machine learning algorithm based on the Vapnik-Chervonenkis (VC) dimension in statistical learning theory and structural risk minimization principle [16]. The flashover voltage prediction is viewed as a binary classification problem in this predictive model. The breakdown or withstanding of an air gap subjected to a given voltage are characterized by 1 and -1. If the critical flashover voltage is U_b, two voltage intervals $[(1-a)U_b, U_b)$ and $[U_b, (1+a)U_b]$ are respectively defined as withstand voltage interval and breakdown voltage interval. a is a percentage to define the voltage interval, a=10% was taken in the present paper. The energy storage features are taken as the input data of the predictive model, while the output data are -1 or 1. Trained by a few known experimental data, the SVM model is used to predict the flashover voltages of air gaps under various conditions. The theoretical basis and the implementation procedures of this prediction method are introduced as follows.

3.1 Brief introduction of SVM

SVM is used as a machine learning technique to solve a classification problem in this paper. It has good generalization performance dealing with small sample and multi-dimensional nonlinear classification problems. Set a known training sample as $T = \{(x_i, y_i)\}$, in which $x_i \in R^k$, $y_i \in \{-1, 1\}$, i=1, 2, ···, n. The implementation of SVM is to solve an optimization problem based on the maximum margin principle, which finds an optimal separating hyperplane to divide the sample data into two diverse classes. By application of the kernel trick, SVM transforms the original sample data into a high dimensional Hilbert space H using nonlinear mapping. The training sample data are transformed to $T_\Phi = \{(\Phi(x_i), y_i)\}$, where $\Phi(x_i) \in H$, $y_i \in \{-1, 1\}$, i=1, 2, ···, n. In this feature space, the sample data can be linearly separated, and the decision function can be expressed as:

$$f(x) = \text{sgn}(w^T \cdot \phi(x_i) + b) \tag{21}$$

where w and b are respectively the weight vector and the bias term of the separating hyperplane, $w \in R^k$ and b is a real number. The symbol "sgn" is the signum function. When $w^T \cdot x_i + b > 0$, the output is 1, while $w^T \cdot x_i + b < 0$, the output is -1. Meanwhile, $w^T \cdot x_i + b = 0$ is the classification hyperplane.

The optimization problem can be expressed as:

$$\begin{cases} \min\limits_{w,b,\xi} & \frac{1}{2}\|w\|^2 + C\sum\limits_{i=1}^{n} \xi_i \\ \text{s.t.} & y_i(w \cdot \phi(x_i) + b) \geq 1 - \xi_i, \quad \xi_i \geq 0, \quad i = 1, 2, \cdots, n \end{cases} \tag{22}$$

where C is the penalty factor which determines the balance between the maximization of the margin and the minimization of the classification error [17].

In order to solve this optimization problem, the Lagrange function is introduced

$$L(w,b,\xi,\alpha,\beta)=\frac{1}{2}\|w\|^2+C\sum_{i=1}^{n}\xi_i-\sum_{i=1}^{n}\alpha_i\{y_i[(w\cdot\phi(x_i))+b]-1+\xi_i\}-\sum_{i=1}^{n}\beta_i\xi_i \tag{23}$$

where $\alpha=(\alpha_1, \ldots, \alpha_n)^T$ and $\beta=(\beta_1, \ldots, \beta_n)^T$ are both the Lagrange multiplier vector. By calculating the partial derivative for w, b and ξ_i, and according to the extremum condition, the following dual problem can be obtained:

$$\begin{cases}\max\limits_{\alpha} & -\frac{1}{2}\sum\limits_{i,j=1}^{n}\alpha_i\alpha_j y_i y_j(\phi(x_i)\cdot\phi(x_j))+\sum\limits_{j=1}^{n}\alpha_j \\ \text{s.t.} & \sum\limits_{i=1}^{n}\alpha_i y_i=0,\quad 0\le\alpha_i\le C,\quad i=1,2,\cdots,n\end{cases} \tag{24}$$

By solving (24), the decision function can be obtained.

It can be seen that the function of transformation Φ is realized by the inner product $(\Phi(x_i)\cdot\Phi(x_j))$. The kernel function can be expressed as:

$$K(x_i,x_j)=(\phi(x_i)\cdot\phi(x_j)) \tag{25}$$

Hence, if the function K is selected, we do not need to choose the transformation Φ. $K(x_i, x_j)$ is used in training and classification instead of $\Phi(x)$. The generalization performance of SVM is determined by properly selecting kernel functions. In this paper, The Gauss kernel is selected as the kernel function of SVM for its good generalization performance and high computational efficiency.

$$K(x_i,x_j)=\exp(-\gamma\|x_i-x_j\|^2),\quad \gamma>0 \tag{26}$$

where γ is the kernel parameter.

The penalty factor C and the kernel parameter γ determine the classification performance of SVM. They are optimized by grid search (GS) method, based on cross validation, to obtain the optimal predictive model [12].

3.2 Golden section search method

The basic idea of the predictive model is to judge whether an air gap will breakdown under a given applied voltage. The corresponding applied voltage under which the output of the model jumps from -1 to 1 is taken as the predicted result of the critical flashover voltage. In order to improve the calculation efficiency, the golden section search method [18] is used to find the flashover voltage.

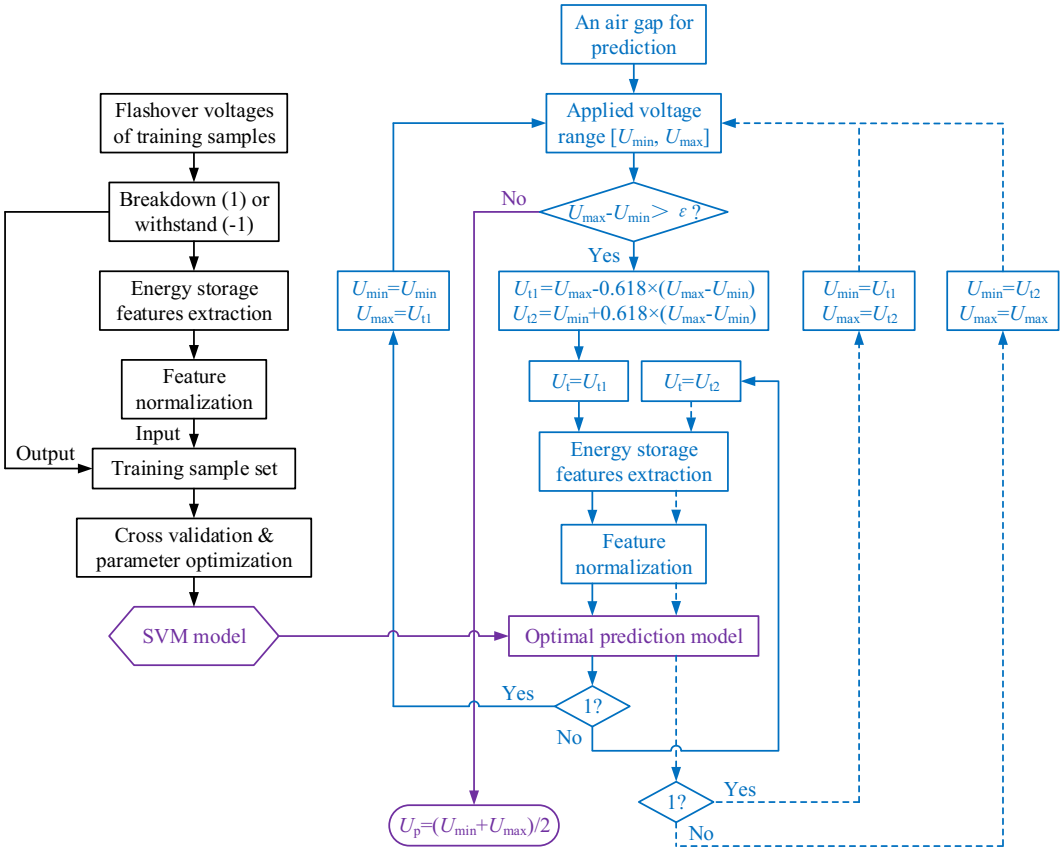

Fig. 2. General flow chart of the prediction method

The search processes of the golden section method are introduced as follows:

(1) The initial search interval for the predicted critical flashover voltage U_p is set as $[U_{min}, U_{max}]$ and the convergence precision is ε. Two voltage values U_{t1} and U_{t2} are inserted into the search interval, $U_{t1}=U_{max}-0.618\times(U_{max}-U_{min})$, $U_{t2}=U_{min}+0.618\times(U_{max}-U_{min})$.

(2) U_{t1} is applied on the air gap for prediction, if the model outputs 1, it means U_{t1} is larger or equal to the critical flashover voltage and therefore the search range of U_p is narrowed to $[U_{min}, U_{t1}]$. If the model outputs -1, it means that U_{t1} is not enough to make the gap breakdown, then U_{t2} is applied on the gap for prediction.

(3) If the model outputs 1 under U_{t2}, then the search range is adjusted to $[U_{t1}, U_{t2}]$. On the contrary, if the model outputs -1, the search scope is narrowed to $[U_{t2}, U_{max}]$.

(4) After multiple iterations, U_{max} and U_{min} are renewed continuously and the search range of U_p is narrowed until $U_{max}-U_{min}<\varepsilon$, then the predicted result of the critical flashover voltage is $U_p=(U_{min}+U_{max})/2$.

3.3 Implementation procedures of the prediction method

The flow chart of the prediction method is shown in Fig. 2. The implementation procedures are depicted as follows.

Firstly, some training samples with known gap geometry and experimental data of flashover voltage are selected to train the SVM model. If the flashover voltage of an air gap is U_b, set the step size as $0.01U_b$, there are 10 voltage values in the withstanding interval $[0.9U_b, U_b)$ and 11 in the breakdown interval $[U_b, 1.1U_b]$. Therefore, a sample can be skillfully extended to 21 data with the applied voltage from $0.9U_b$ to $1.1U_b$, and their output data are -1 and 1.

Secondly, energy storage features of each training sample are extracted from the FEM calculation results of the electric field distribution, and calculated by solving the constraint equations of the impulse voltage waveform. These features are normalized to [0, 1] by:

$$\overline{x}_i = \frac{x_i - x_{min}}{x_{max} - x_{min}} \tag{27}$$

where x_i is a feature and $\overline{x}_i$ is its normalized value, x_{min} and x_{max} are respectively the minimum and maximum value of x_i. After normalization, the energy storage features are taken as the input data to train the SVM model. Based on cross validation, the optimal penalty factor C and kernel parameter γ are searched by GS method. Trained by the known experimental data, SVM establishes the multi-dimensional nonlinear relationship between the flashover voltages of air gaps and their energy storage features.

Thirdly, the optimal SVM model is used to predict the flashover voltages of test samples. For an air gap, the estimated critical flashover voltage is set in the range $[U_{min}, U_{max}]$, the predicted result is searched by the golden section search method. For each applied voltage, the energy storage features are extracted and input to the predictive model to judge whether the output is -1 or 1. For example, the first applied voltage is $U_{t1}=U_{max}-0.618\times(U_{max}-U_{min})$, then the energy storage features of this air gap are calculated under U_{t1} and input to the trained SVM model. According to the output of the model, namely, 1 or -1, the search interval will be narrowed to $[U_{min}, U_{t1}]$ to generate another applied voltage value, or otherwise, U_{t2} is applied to calculate the energy storage features which will be input to the predictive model to judge whether the output is -1 or 1. So repeatedly, the search interval is eliminated constantly and the iterative computations are conducted until the convergence condition $U_{max}-U_{min}<\varepsilon$ is satisfied. The flashover voltage prediction result is the average value of the last two applied voltages.

4. Lightning Impulse Flashover Voltage Prediction of Typical Air Gaps

The proposed predictive model is used to predict the lightning impulse flashover voltages of air gaps with various geometries and under different lightning impulse voltage waveshapes, thus to verify the validity of the proposed energy storage features and the flashover voltage prediction method.

4.1 Training and test samples

The lightning impulse discharge tests of rod-rod air gaps were carried out by the AIEE in 1930s, under the waveforms of 1/5 μs and 1.5/40 μs [19]. The experimental data given in [19] were obtained under the atmospheric environment of t=25℃, p=101.3 kPa and h=15 g/m^3. These data were corrected to standard atmospheric conditions by g parameter method recommended in IEC 60060-1 [15]. IEEE Standard 4-1995 [20] recommends the arrangement of a rod-rod gap for voltage measurement, as shown in Fig. 3, and gives the critical sparkover voltages of these rod-rod gaps with different gap lengths, subjected to the lightning impulse voltages of 1.2/5 μs and 1.2/50 μs. These voltage values are under standard atmospheric conditions. The rod gap consists of two 12.5 mm square rod electrodes arranged horizontally. The experimental results under positive lightning impulses were taken as sample data to validate the validity of the prediction method.

In order to make the predictive model generalize to various gap configurations and voltage waveforms, the selected training sample set contains the experimental data of rod-rod gaps with different gap lengths and voltage waveforms, as shown in Table 1, altogether 7 samples. Other gaps with various conditions were taken as test samples for flashover voltage prediction and the predicted

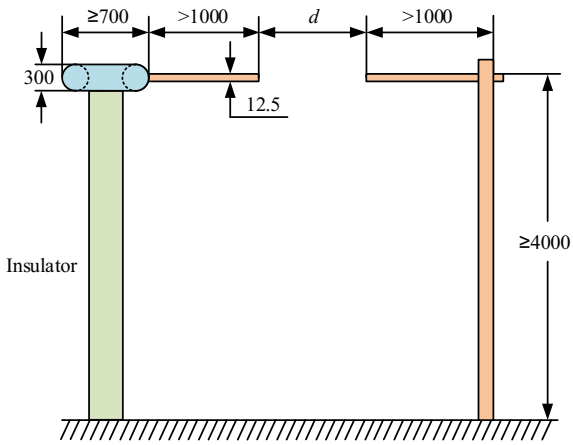

Fig. 3. Arrangement of the standard rod-rod gap (all dimensions are in millimeters)

Table 1. Training sample set

Impulse waveform	*d* (cm)	*U* (kV)	Impulse waveform	*d* (cm)	*U* (kV)
1.2/50 μs	20	157.5	1.2/5 μs	30	277
	50	339	1.5/40 μs	76.2	496.7
	100	625	1/5 μs	127	1039
	140	850	—	—	—

results were compared with the experimental data obtained by IEEE Standard 4-1995 and AIEE. There are altogether 38 test samples of rod-rod gaps, whose gap lengths range from 20 cm to 152.4 cm, and the applied voltages contain the above-mentioned 4 waveforms. Furthermore, in order to validate the generalization performance for other gap types, 7 samples of sphere-plane under 1/50 μs lightning impulse [21] and 4 samples of rod-plane gap under 1.2/50 μs waveshape [22] were also taken as the test samples. For the sphere-plane gap, the sphere diameter is 2.5 cm and the plane electrode is a 60 cm diameter disc, the gap length ranges from 10 cm to 50 cm. The experimental data of sphere-plane gaps were obtained under normal laboratory atmospheric conditions and no correction was made [21]. The rod-plane gap consists of a cylindrical brass rod with a hemispherical tip and a grounded aluminium plane, the rod diameter is 2.2 cm, and the size of the plane electrode is 100 cm×200 cm. The data of rod-plane gaps were corrected to standard atmospheric conditions. The experimental data of the above-mentioned test samples are shown in Table 2, where *d* is the gap length and *U* is the critical flashover voltage.

According to the parameters shown in Fig. 3, the three dimensional finite element models of the standard rod-rod gaps with different gap lengths were established by ANSYS software, and their electrostatic field distributions were calculated. Taking the 30 cm gap for example, the high-voltage rod electrode was applied unit voltage 1 V and the grounded rod was applied 0 V, its electric field distribution is shown in Fig. 4. The discharge channel is a square region between two electrodes, the length of side is

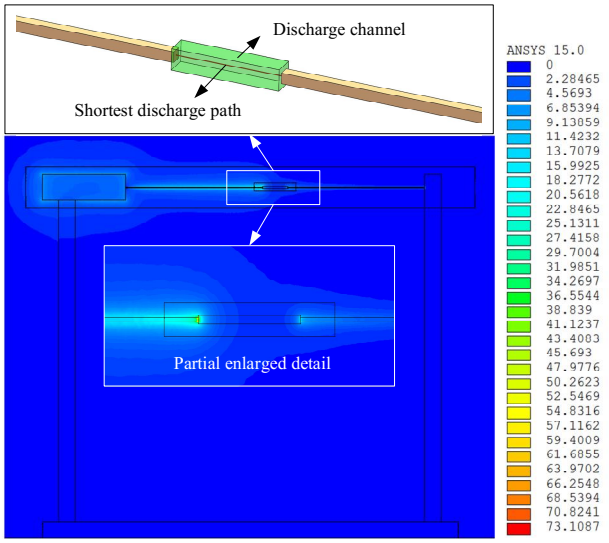

Fig. 4. The electric field distribution of the standard rod-rod gap (*d*=30 cm) and the schematic diagram of the discharge channel and the shortest discharge path

Table 2. Experimental data of test samples

Rod-rod (1.2/50 μs)		Rod-rod (1.2/5 μs)		Rod-rod (1.5/40 μs)	
d (cm)	*U* (kV)	*d* (cm)	*U* (kV)	*d* (cm)	*U* (kV)
25	184	20	188	20.32	162.9
30	217	25	234	22.86	176.3
35	250	35	320	25.4	189.3
40	281	40	362	38.1	273.0
45	309	45	405	50.8	345.8
60	392	50	445	101.6	636.9
70	450	60	525	127	782.5
80	510	70	605	152.4	922.7
90	570	80	690	Rod-rod (1/5 μs)	
120	735	90	765	*d* (cm)	*U* (kV)
Sphere-plane (1/50 μs)		100	845	20.32	189.4
d (cm)	*U* (kV)	120	990	25.4	235.9
10	65	140	1150	38.1	343.7
15	90	Rod-plane (1.2/50 μs)		50.8	443.8
20	113	*d* (cm)	*U* (kV)	76.2	644.1
25	140	12.5	95	101.6	838.8
30	170	25	163	152.4	1233.8
40	235	37.5	223	—	—
50	267	50	278		

twice that of the rod electrode. For the hemispherical rod-plane and sphere-plane configurations, the discharge channel is the cylindrical region between the rod or sphere electrode and the plane electrode, and the radius of the cylinder is the same with the rod or sphere electrode.

By post-processing of the FEM calculation results, the original data related to the electric field were extracted, and the electric field features of each sample were calculated according to their definitions. In addition, the double exponential functions of the lightning impulses with different waveshapes can be solved by their constraint equations. Therefore, the impulse voltage waveform features of each sample can be obtained according to their calculation formulas.

4.2 Predicted results and analysis

The optimal penalty factor C and kernel parameter γ were searched by GS method based on 3-fold cross validation. The training samples were divided into 3 groups for cross validation. The search scopes and step sizes of C and γ were firstly determined for mesh generation, and the classification accuracies of the SVM model under different values of C and γ were compared with each other. The C and γ under which the SVM has the best prediction results for training samples were selected as the optimal parameters of the predictive model. In this paper, the SVM parameter optimization result by GS method is shown in Fig. 5. It can be seen that the optimal C=103.97, γ=0.095, under which the best cross validation accuracy for the training samples is 98.64%. The trained SVM model was used to predict the critical flashover voltages of the test samples. The initial range of the applied voltage was set as U_{min}= 0 kV and U_{max}=1500 kV. The convergence precision ε was set as 1 kV. After multiple iterative computations by golden section search method, the predicted results could be obtained.

The critical flashover voltage of every sample was predicted one by one, for each gap length and voltage waveform. Fig. 6 summarizes the comparison of the flashover voltage prediction results of rod-rod gaps with the experimental values obtained by IEEE Standard 4-1995 and AIEE. For better comparisons, the predicted results of the training samples were also plotted in Fig. 6. It can be seen that the predicted values of the flashover voltage correlate well with the experimental data. The predicted results of all the test samples, under 4 different lightning impulse waveforms, have high accuracy. The relative errors of the predicted values are within 8% for most of the test samples, which are acceptable for engineering applications. It should be noted that the experimental data also have certain errors or dispersions [25].

The comparison of the flashover voltage prediction results of rod-plane and sphere-plane gaps with the experimental data is shown in Fig. 7. The predicted values of sphere-plane gaps under 1/50 μs impulse agree well with the test results, and the relative errors are within 5%. The predicted results of rod-plane gaps under 1.2/50 μs impulse diverge a little from the experimental data in trend, but the relative errors are also within acceptable range. The errors may be caused by different atmospheric conditions and correction methods between the experimental results of rod-plane gaps and the training samples.

The following 3 common error indexes were used to evaluate the prediction accuracy of the SVM model.

$$e_{\mathrm{RMSE}} = \sqrt{\frac{1}{N}\sum_{i=1}^{N}[U_{\mathrm{t}}(i)-U_{\mathrm{p}}(i)]^2} \tag{28}$$

$$e_{\mathrm{MAPE}} = \frac{1}{N}\sum_{i=1}^{N}\left|\frac{U_{\mathrm{t}}(i)-U_{\mathrm{p}}(i)}{U_{\mathrm{t}}(i)}\right| \tag{29}$$

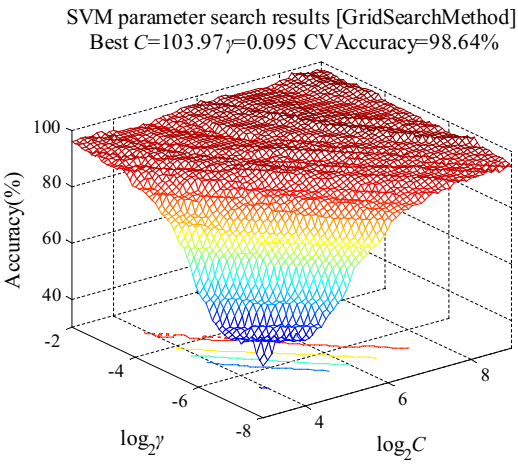

Fig. 5. SVM parameter optimization results of C and γ by grid search method

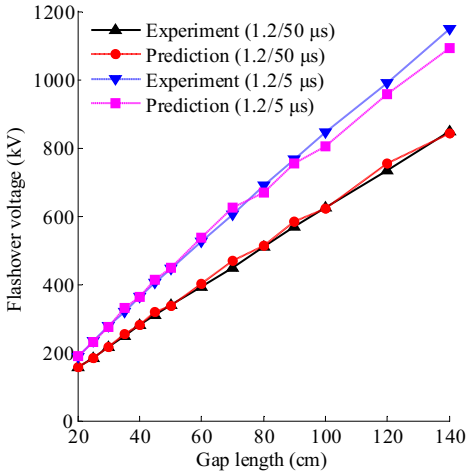

(a) Comparison with IEEE Standard 4-1995 results

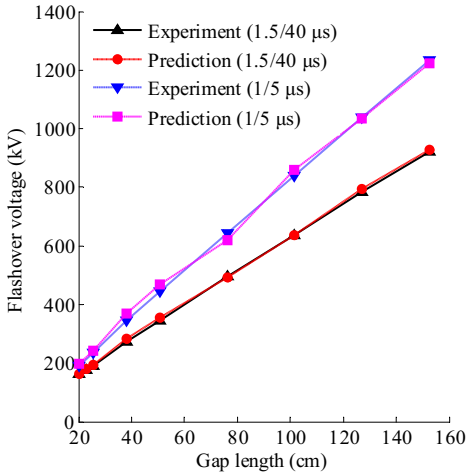

(b) Comparison with AIEE results

Fig. 6. Comparison of the flashover voltage prediction results of rod-rod gaps with the experimental data

Table 3. Error indexes of the predicted results

Error indexes	Rod-rod				R-P	S-P
	1.2/50 μs	1.2/5 μs	1.5/40 μs	1/5 μs	1.2/50 μs	1/50 μs
e_{MSE}	10.94	23.89	6.56	18.28	7.94	6.54
e_{MAPE}	0.019	0.025	0.015	0.037	0.046	0.042
e_{MSPE}	0.007	0.008	0.007	0.016	0.027	0.018

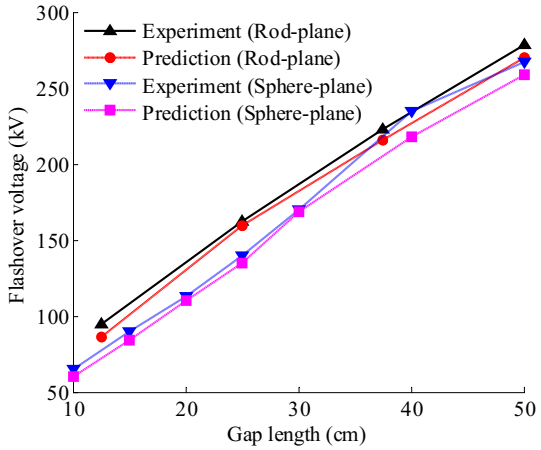

Fig. 7. Comparison of the flashover voltage prediction results of rod-plane and sphere-plane gaps with the experimental data

$$e_{MSPE} = \frac{1}{N}\sqrt{\sum_{i=1}^{N}\left[\frac{U_t(i)-U_p(i)}{U_t(i)}\right]^2} \quad (30)$$

where $U_t(i)$ and $U_p(i)$ are respectively the trial and predicted flashover voltage of the ith test sample, N is the number of the test samples. e_{RMSE} is the root mean square error, e_{MAPE} is the mean absolute percentage error, and e_{MSPE} is the mean square percentage error. The three error indexes of the predicted results of different gap types and under different voltage waveforms are summarized in Table 3. The e_{MAPE}s of rod-rod gaps under 1.2/50μs, 1.2/5μs, 1.5/40 μs, and 1/5 μs are respectively 1.9%, 2.5%, 1.5% and 3.7%. For rod-plane (R-P) and sphere-plane (S-P) gaps, their e_{MAPE}s are 4.6% and 4.2%. The error analysis results demonstrate the validity and accuracy of the proposed method for lightning impulse flashover voltage prediction of various gap configurations.

5. Discussions

The flashover voltage is the most important parameter for the determination of gap arrangements and insulation coordination in engineering practice. The proposed method provides an alternative way to study the air gap discharge instead of paying attention to the complex physical processes. The successful implementation of lightning impulse flashover voltage prediction of air gaps by SVM model is an innovative applications of modern mathematical methods to solve the traditional problems in the area of high voltage engineering. During the past few decades, a large number of experimental data about the flashover voltages of air gaps with various configurations have been accumulated worldwide. If these data can be utilized for machine learning reasonably, it may be useful to predict the flashover voltages of air gaps with new geometry, which helps to reduce the required test work for insulation design of high voltage equipment.

Further studies are still necessary to be carried out to improve this model, and the applications of this model on air gaps used in practical engineering are another research content in the subsequent studies. It may provide reference for insulation designs of some actual equipment. The lightning impulse flashover voltage prediction in this paper involves different gap structures including rod-rod, sphere-plane and rod-plane gaps, and the good prediction results preliminarily verify the generalization performance of this approach for different geometry of electrodes. The purpose of characterizing the gap geometry by electric field features is to generalize this approach to different gap structures. For example, the 50% flashover voltage prediction of parallel gaps installed on insulator strings for lightning protection may be an interesting and useful topic. Furthermore, except for the flashover voltage, the volt-time characteristic of an air gap under lightning impulse is also of important practical significance for application purpose. How to predict the voltage-time curve by this model is another challenge to be overcome in the future.

6. Conclusion

A numerical approach to predict the lightning impulse flashover voltages of air gaps based on energy storage features and SVM is proposed in this paper. The impulse voltage waveform features and electric field features are defined to characterize the temporal accumulation and spatial distribution of the capacitive energy applied on an air gap, and they are taken as the input data of the SVM model. The golden section search method is used to efficiently predict the critical flashover voltage under an applied voltage range.

The positive lightning impulse flashover voltages of rod-rod, rod-plane and sphere-plane gaps are predicted by the SVM model, considering different waveshapes and gap lengths. The predicted results are in good accordance with the experimental data, with the same trends and acceptable errors. The mean absolute percentage errors of rod-rod gaps under 4 different waveforms are respectively 1.9%, 2.5%, 1.5%, and 3.7%, while for rod-plane and sphere-plane gaps, they are 4.6% and 4.2%. The results indicate the feasibility of the proposed method for air gap flashover voltage prediction under lightning impulses. This method provides an alternative way for prediction study of air gap

breakdown characteristics with various gap geometries and voltage waveforms, therefore helps to estimate the safe clearances of air gaps for insulation design and contributes to reducing the required test work.

Acknowledgements

This work is supported by China Postdoctoral Science Foundation (2016M602354) and the Fundamental Research Funds for the Central Universities (2042017kf1009, 2042018kf0020).

References

[1] D. C. Huang, Y. B. Shu, J. J. Ruan and Y. Hu, "Ultra high voltage transmission in China: developments, current status and future prospects," *Proc. IEEE*, vol. 97, no. 3, pp. 555-583, Mar. 2009.

[2] S. Chen, R. Zeng and C. J. Zhuang, "The diameters of long positive streamers in atmospheric air under lightning impulse voltage," *J. Phys. D: Appl. Phys.*, vol. 46, no. 37, pp. 375203, Sep. 2013.

[3] X. G. Zhao, J. J. He and H. X. He, "Effect of branching on spikes of positive leader current," *IEEE Trans. Dielectr. Electr. Insul.*, vol. 23, no. 4, pp. 1968-1973, Aug. 2016.

[4] N. Goelian, P. Lalande, A. Bondiou-Clergerie, G. L. Bacchiega, A. Gazzani and I. Gallimberti, "A simplified model for the simulation of positive-spark development in long air gaps," *J. Phys. D: Appl. Phys.*, vol. 30, no. 17, pp. 2441-2452, Sep. 1997.

[5] L. Arevalo, D. Wu and B. Jacobson, "A consistent approach to estimate the breakdown voltage of high voltage electrodes under positive switching impulses," *J. Appl. Phys.*, vol. 114, no. 8, pp. 083301-083308, Aug. 2013.

[6] J. H. Rakotonandrasana, A. Beroual and I. Fofana, "Modelling of the negative discharge in long air gaps under impulse voltages," *J. Phys. D: Appl. Phys.*, vol. 41, no. 10, pp. 105210-105224, May 2008.

[7] A. Beroual, J. H. Rakotonandrasana and I. Fofana, "Predictive dynamic model of the negative lightning discharge based on similarity with long laboratory sparks – part 1: physical process and modeling," *IEEE Trans. Dielectr. Electr. Insul.*, vol. 17, no. 5, pp. 1551-1561, Oct. 2010.

[8] L. Arevalo and V. Cooray, "Preliminary study on the modelling of negative leader discharges," *J. Phys. D: Appl. Phys.*, vol. 44, no. 31, pp. 315204, Aug. 2011.

[9] CIGRE Working Group 33.07, "Guidelines for the evaluation of the dielectric strength of external insulation," Int. Council Large Electric Systems (CIGRE), Paris, France, Tech. Brochures 72, 1992.

[10] S. A. Boggs, T. Uchii and S. Nishiwaki, "Analytical approach of SF_6 breakdown under transient conditions," *IEEE Trans. Power Del.*, vol. 18, no. 3, pp. 751-757, Jul. 2003.

[11] Z. B. Qiu, J. J. Ruan, D. C. Huang, Z. H. Pu and S. W. Shu, "A prediction method for breakdown voltage of typical air gaps based on electric field features and support vector machine," *IEEE Trans. Dielectr. Electr. Insul.*, vol. 22, no. 4, pp. 2125-2135, Aug. 2015.

[12] Z. B. Qiu, J. J. Ruan, D. C. Huang, M. T. Wei, L. Z. Tang, C. P. Huang, W. J. Xu and S. W. Shu, "Hybrid prediction of the power frequency breakdown voltage of short air gaps based on orthogonal design and support vector machine," *IEEE Trans. Dielectr. Electr. Insul.*, vol. 23, no. 2, pp. 795-805, Apr. 2016.

[13] Z. B. Qiu, J. J. Ruan, C. P. Huang, W. J. Xu, L. Z. Tang, D. C. Huang and Y. F. Liao, "A method for breakdown voltage prediction of short air gaps with atypical electrodes," *IEEE Trans. Dielectr. Electr. Insul.*, vol. 23, no. 5, pp. 2685-2694, Oct. 2016.

[14] Z. B. Qiu, J. J. Ruan, D. C. Huang, S. W. Shu and Z. Y. Du, "Prediction study on positive DC corona onset voltage of rod-plane air gaps and its application to the design of valve hall fittings," *IET Gener. Transm. Distrib.*, vol. 10, no. 7, pp. 1519-1526, May 2016.

[15] IEC 60060-1, "High-voltage test techniques – part 1: general definitions and test requirements," 2010.

[16] V. N. Vapnik, "Methods of pattern recognition," in The Nature of Statistical Learning Theory, 2nd ed., New York: Springer-Verlag, 2000, pp. 138-146.

[17] S. Abe, "Two-class support vector machines," in Support Vector Machines for Pattern Classification, 2nd ed., London: Springer-Verlag London Limited, 2010, pp. 28-31.

[18] J. Alikhani Koupaei, S. M. M. Hosseini and F. M. Maalek Ghaini, "A new optimization algorithm based on chaotic maps and golden section search method," *Eng. Appl. Artfl. Intell.*, vol. 50, pp. 201-214, Apr. 2016.

[19] The subcommittee on correlation of laboratory data of EEI-NEMA joint committee on insulation co-ordination, "Flashover characteristics of rod gaps and insulators," *Trans. AIEE*, vol. 56, no. 6, pp. 712-714, Jun. 1937.

[20] IEEE Standard 4, "IEEE standard techniques for high-voltage testing," 1995.

[21] M. Abdullah and E. Kuffel, "Development of spark discharge in nonuniform field gaps under impulse voltages," *Proc. IEE*, vol. 112, no. 5, pp. 1018-1024, May 1965.

[22] P. N. Mavroidis, P. N. Mikropoulos and C. A. Stassinopoulos, "Discharge characteristics in short rod-plane gaps under lightning impulse voltages of both polarities," in *Proceedings of the 42nd Intl. Univ. Power Eng. Conf.*, 2007, pp. 1070-1074.

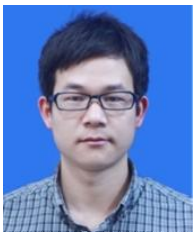

Zhibin Qiu He received the B.S. degree in electrical engineering and automation, and the Ph.D. degree in high voltage and insulation technology from the School of Electrical Engineering, Wuhan University, Wuhan, China in 2011 and 2016, respectively, where he is currently engaged in postdoctoral research. His research interests include air gap discharge characteristics, high voltage and insulation technology.

Jiangjun Ruan He received the B.S. and Ph.D. degrees in electric machine engineering from Huazhong University of Science & Technology, Wuhan, China in 1990 and 1995, respectively, and finished his post-doctoral research from Wuhan University of Hydraulic & Electric Engineering, Wuhan, China in 1998. He is currently a Professor of Wuhan University, Wuhan, China. His research interests include electromagnetic field calculation, high voltage and insulation technology.

Congpeng Huang He received the B.S. degree in electrical engineering and automation from the School of Electrical Engineering, Wuhan University, Wuhan, China in 2015, where he is pursuing the Master degree in electrical engineering. His research interests include numerical calculation of electromagnetic field, high voltage and insulation technology.

Wenjie Xu She received the B.S. degree in electrical engineering and automation from the School of Electrical Engineering, Wuhan University, Wuhan, China in 2015, where she is pursuing the Master degree in electrical engineering. Her research interests include numerical calculation of electromagnetic field, high voltage and insulation technology.

Daochun Huang He received the B.S. and Ph.D. degrees in high voltage and insulation technology from the School of Electrical Engineering, Wuhan University, Wuhan, China in 2003 and 2009, respectively. Currently, he is an Associate Professor with the School of Electrical Engineering, Wuhan University. He is a member of IEEE Dielectrics and Electrical Insulation Society (DEIS) and the International Council on Large Electric Systems (CIGRE). His research interests include external insulation of transmission and transformation equipment, high voltage apparatus, numerical analysis of electromagnetic field and its applications in engineering.